3D-Printing, Topology Optimization and Statistical Learning: A Case Study

Vishu Bhooshan[1], **Mathias Fuchs**[1] **and Shajay Bhooshan**[1]

[1]Zaha Hadid Architects, Computation & Design Research Group (ZH_CODE)
10 Bowling Green Lane London, UK EC1R 0BQ
{firstname.lastname}@zaha-hadid.com

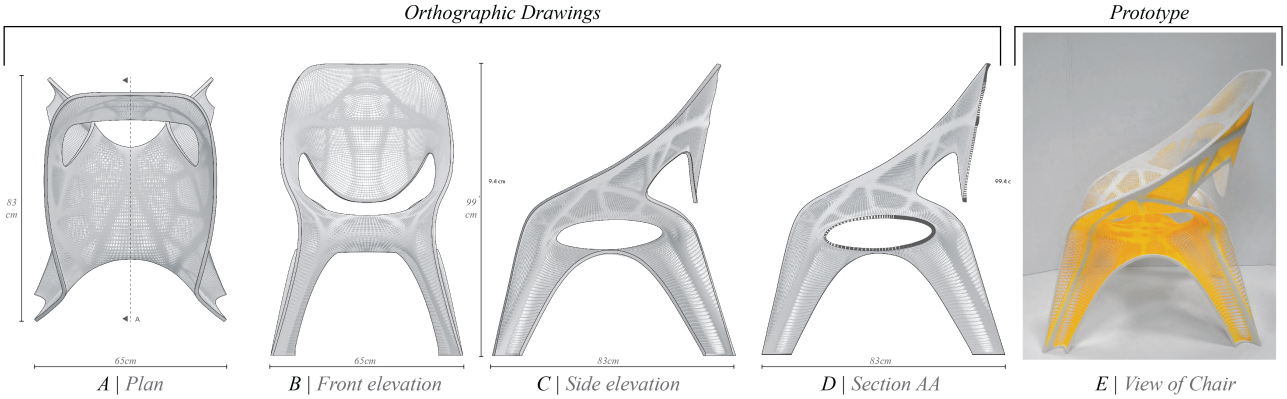

Figure 1: The Chair Prototype

ABSTRACT

This research paper explores the use of 3D-printing technologies in prototyping of Topology Optimization (TO) driven design. The paper describes the integration of TO into an early design work-flow and highlights the difficulties thereof. Due to the high computation times of TO, we outline the use of statistical learning to approximate TO material density results. Specifically, we highlight the use of such techniques for TO of thin-shell, minimal surface chair geometries and the incorporation of specific assumptions related to such geometries to improve the functional approximation using statistical methods. We describe the various stages of the design pipeline that benefit from interactive TO.

Author Keywords

topology optimization; 3D-printing; statistical learning; work-flows & digital tools; interactive editing; edit-and-observe;

1 INTRODUCTION

3D-printing, a layer-by-layer additive manufacturing technique [**?**] is typically used to deliver geometrically precise, functional prototypes in a short period of time. It has emerged as one of the key rapid prototyping technologies in the field of product design [**?**] and in large scale architectural design [**?**, **?**]. Large 3D-printing companies such as Stratasys [**?**] most commonly use thermoplastics - *ABS* (Acrylonitrile-Butadiene Styrene) / *PLA* (PolyLactic Acid) - as a material. There have been several recent attempts to investigate alternate materializations like clay & concrete [**?**], resin & metal [**?**], glass [**?**] etc. This along with the development in higher precisions and larger build volumes [**?**] makes 3D-printing conducive to realize customized designs. Topology Optimization (TO), a field of structural mechanics [**?**] has found increased application in architectural design in recent times [**?**, **?**, **?**]. Its use in architectural design is characterized by the outcome of the simulation being dominantly and visually expressed in the final design. Due to the complexity and intricacy of the results, TO is often constrained to research studies [**?**]. 3D printing has been used increasingly to materialize TO driven designs [**?**, **?**, **?**].

TO faces similar challenges of computational time as other Finite Element Method based simulations, making it unsuitable for interactive edit-and-observe design methods preferred by designers. Statistical learning techniques have been previously applied to alleviate similar problems in Computational Fluid Dynamics [**?**]. Additionally, there are several examples of using domain specific information to improve the accuracy of the approximation [**?**]. The use of statistical learning to approximate TO results along with successful realization of TO driven design prototypes with 3D-printing are the primary contributions of this paper.

2 PAPER ORGANIZATION

The paper is prompted by the experiences of using TO for the design and manufacture of a chair (Figure 1) using high-resolution 3D-printing technologies. Section **??** outlines the various stages of the design work-flow that incorporates and highlights the benefits of using procedural modeling of design geometry, TO for structural evaluation and material saving results, re-meshing to produce a structurally aligned geometry and preparation of the geometry for production. In

SimAUD 2017 May 22-24 Toronto, Canada © 2017 Society for Modeling & Simulation International (SCS)

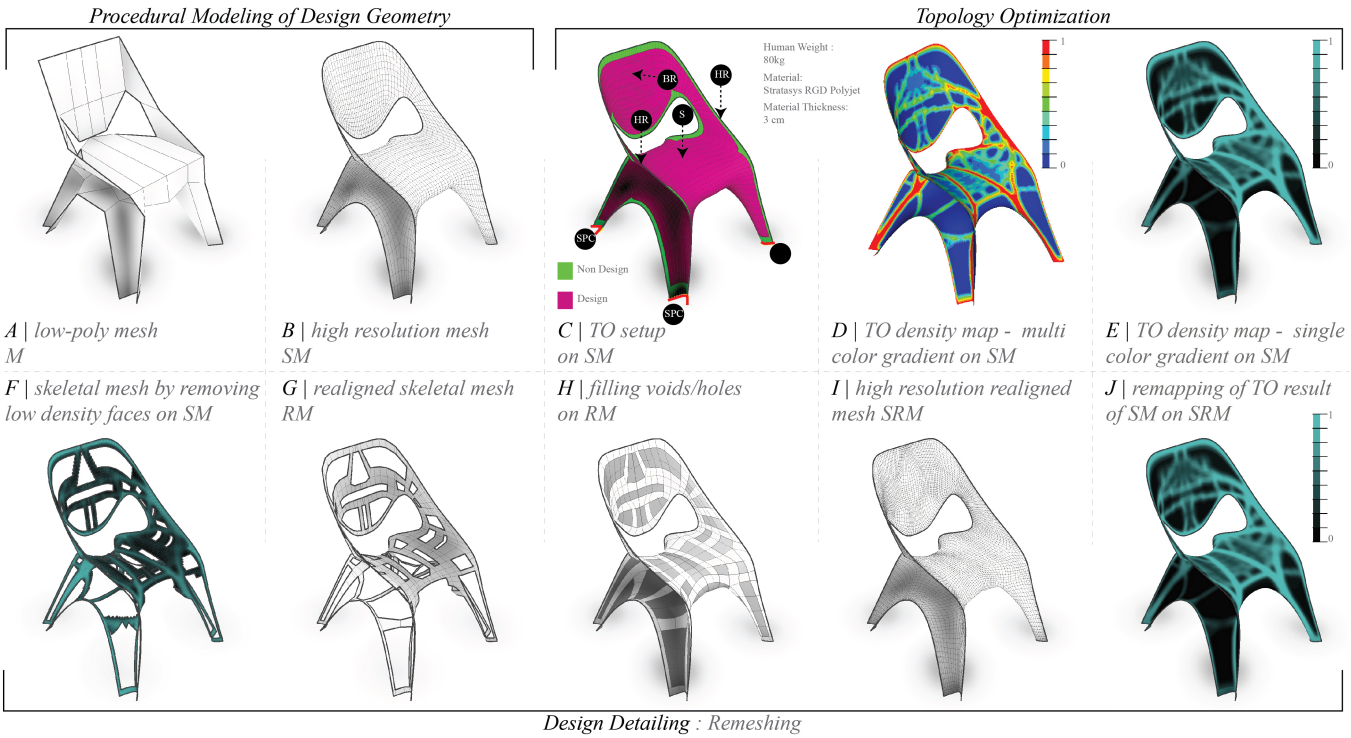

Figure 2. Procedural Modeling, Topology Optimization, and Re-meshing

Section **??**, we discuss the motivation for using statistical learning to approximate TO results and explain the variables, methods and prediction results. We comment on the extension of the work in both the 3D-printing and statistical learning domain in Section **??**.

3 DESIGN WORK-FLOW

The design work-flow consists of five steps, each of which is described in subsequent subsections.

1. Procedural modeling of design geometry
2. Topology Optimization
3. Re-meshing
4. Parametric design detailing
5. Generating production information

3.1 Procedural Modeling of Design Geometry

Initially, using the process of hierarchical subdivision surface modeling [**?**], a *low-poly mesh* (M) (Figure **??**A) is defined. A manifold M that is predominantly represented by a *quad-faced mesh* lends itself to ease of manipulation of the design geometry and hence helps in creating multiple and quick design iterations. The desired M is then subdivided using the modified Catmull-Clark subdivision scheme inbuilt into Autodesk Maya [**?**] to create a *high-resolution mesh* (HR-M) (Figure **??**B). This improves results from the next step of TO. An iterative perturbation scheme — the so-called *dynamic relaxation* method [**?**] is applied to HR-M in order to get an even distribution of quads(Figure **??**C).

3.2 Topology Optimization

TO is usually addressed under the heads of size, shape and topology [**?**]. Each of these have been well researched and documented. For comprehensive understanding on shape optimization, we refer the reader to [**?**], [**?**], [**?**] and to [**?**], [**?**] for size optimization.

In this paper we refer to TO by the *homogeneous method* defined as a *distribution problem of isotropic material* which addresses all three aspects of size, shape and topology simultaneously [**?**]. Given a set of design constraints, support conditions, applied loads, thickness/volume of material, TO is used to *find the optimal layout of a material densities within a specified region* [**?**]. We have used the *Optistruct* [**?**] and its proprietary optimization algorithm inbuilt in Altair Hypermesh to run the TO simulations.

The process of TO begins by defining the *design and non-design area*. The non-design areas are frozen from the optimization. For the chair, all of the *boundary faces* of HR-M are defined as non-design area and the rest of the faces as design area. All the base *boundary vertices* of HR-M are defined as the support condition which are called as *Single Point Constraints* (SPC). The loads were applied considering an 80 kg human seated on the chair and were classified as load on *seat* (S), *back-rest* (BR) and *hand-rest* (HR) (Figure **??**C). The mechanical properties of the material used correspond to the specifications provided by Stratasys - *RGD Polyjet Plastic* [**?**]. The maximum thickness constraint imposed on the optimization of the chair was 3cm.

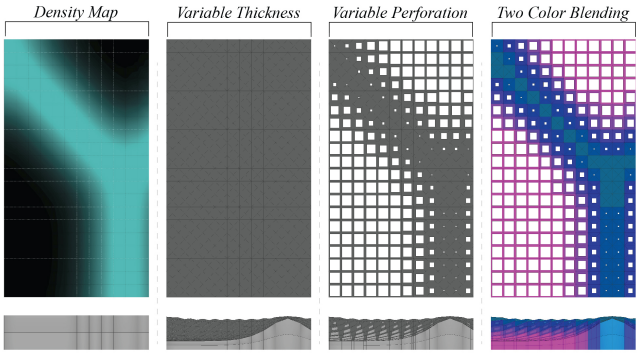

Figure 3. Parametric Design Detailing

3.3 Re-meshing

After the TO simulation , the material distribution map (multi-color gradient) (Figure **??**D) showing *material density* per vertex of HRM is converted into a single color gradient (Figure **??**E). The density value per vertex varies in the domain of 0 (potential void) to 1 (structural member) [**?**]. We do a *Re-meshing* of HR-M since the *mesh-edges* of HR-M do not align with the gradient of the TO material density map. A skeletal *Realigned Mesh* (RM) is created using the high material density area of HR-M (Figure **??**F-G). Next, the holes of RM (Figure **??**H) are filled and converted into a *high-resolution Realigned mesh* (HR-RM) (Figure **??**I). The single-color gradient density values of HR-M are then mapped back onto HR-RM (Figure **??**J).

3.4 Parametric design detailing

Subsequently, a bespoke algorithm utilizes the material-density information on HR-RM, to create another mesh with varying thickness and perforation (DM) (Figure **??**). For the chair, the thickness varies from 3 cm to 1 cm for corresponding vertex density value of 1 and 0 respectively. The perforation were created per face (density value per face computed as average density of all the vertices attached to that face) and the size of the perforation was a percentage of the area of the face. This percentage varied from 0 to 75% for corresponding face density value of 1 and 0 respectively. Since the Stratasys printer could do multi-colored print, the same data of vertex density value are used to create a blend between two user input colors (Figure **??**). This process of varying the thickness results in a material saving of 40% in comparison to a geometry of uniform thickness of 3cm. This saving increases to 55%, when thickness and perforation sizes are varied simultaneously.

3.5 Production

The information needed by the 3D-printer was extracted to suit the prevalent industry standard of partitioning design geometry into shells / solids of constant material properties [**?**]. The number of shells is a function of the number of colors used in the design of the chair (Figure **??**) - *single-color gradient chair* (10 shells), *multi-color gradient chair* (20 shells), *single-color chair* (1 shell).

4 APPROXIMATING RESULTS OF TO

TO, as noted in the Section 1, is expensive in terms of computational time. Since the time required to achieve these accurate results is greater than that available in a design work-flow it becomes difficult to integrate TO at the early stage of the design work flow [**?**]. As such, quick qualitative results that provide interactive feedback to the designer are just as important as the accurate, material-saving results. In order to overcome this difficult , we looked at statistical learning algorithms to approximate TO results with domain specific data such as *principal curvatures, vertex normals* etc which areadditionall intrinsic properties of the design geometry. Here, we briefly outline our thinking behind the heuristic that was used as part of the statistical learning method. Let us briefly assume the surface to be *funicular*. Then, it is a commonly used approximation to apply the equation describing a deflected membrane stretched by a transverse load ([**?**, Equation 9.16]). By funicularity, the membrane under pure tension gets inverted "upside down" to a pure compression shell. Thus, we view the surface as a solution of $\Delta z = -w$ where z is the height function of the two variables x, y that parametrise the projection onto the $x - y$ plane, and w denotes the applied load. Furthermore, it is well known that the structural properties of a surface can be expressed in terms of the Airy stress function ϕ such that

$$\frac{\partial^2\phi}{\partial y^2}\frac{\partial^2 z}{\partial x^2} - 2\frac{\partial^2\phi}{\partial x\partial y}\frac{\partial^2 z}{\partial x\partial y} + \frac{\partial^2\phi}{\partial x^2}\frac{\partial^2 z}{\partial y^2} = -w \qquad (1)$$

([**?**, 3.2.1]) with a function ϕ of x and y. Taking these equations together, one can see that the Airy potential of an equilibrium, compression-only surface can approximately assumed to be the paraboloid $\phi(x, y) = (x^2 + y^2)/2$ because its *Hessian matrix* is the unit matrix. Then, (**??**) simplifies to $\Delta z = -w$. Let us from now on abbreviate the partial derivatives with a subscript. There is the relationship $S = (\sqrt{\det g})g^{-1}\sigma$ ([**?**] and the corrected version [**?**]) between $S = \begin{pmatrix} \phi_{yy} & -\phi xy \\ -\phi xy & \phi_{xx} \end{pmatrix}$, the metric $g = \begin{pmatrix} 1+z_x^2 & z_x z_y \\ z_x z_y & 1+z_y^2 \end{pmatrix}$, and the stress tensor σ. For the particular case where the Airy stress potential is given by paraboloid, the matrix S reduces to the unit matrix. We obtain an approximate explicit formula $\sigma = (\sqrt{\det g})^{-1} g$ or

$$\sigma = \frac{1}{\sqrt{1 + z_x^2 + z_y^2}} \begin{pmatrix} 1+z_x^2 & z_x z_y \\ z_x z_y & 1+z_y^2 \end{pmatrix}, \qquad (2)$$

expressing the stress tensor in purely local geometric terms. To illustrate this thought by an example, let us suppose, for instance, that the structure is a linear protrusion along the y-axis of a shape that varies only along the x-axis, and the surface is subjected to self-load so that $w = \sqrt{1 + z_x^2 + z_y^2}$. Then, $z_y = 0$, and (**??**) means that the compression in a catenary arch satisfies $\sigma = \begin{pmatrix} \cosh(x) & 0 \\ 0 & 0 \end{pmatrix}$ in accordance with well-known

Figure 4. Production Information for 3D-Printing

theory on catenaries and funicular arches [**?**].
One can prove that the "true" stress tensor $\boldsymbol{\sigma}$ seen as a linear self-maps of the tangent vector space to the structure at any interior point and σ are related by the intertwining relation $\boldsymbol{\sigma} = dz\ \sigma\ (dz)^{-1}$ where dz is the differential of z as a function of x and y. Thus, the eigenvalues of $\boldsymbol{\sigma}$ and σ agree.
Taking these thoughts together, the principal stresses of a compressive structure in equilibrium are approximately the eigenvalues of (**??**), which are quickly calculated and given by $\lambda_1 = \sqrt{1 + z_x^2 + z_y^2}$, $\lambda_2 = (\lambda_1)^{-1}$. Thus, the principal stresses and their directions are given in terms of the local geometry, bypassing the need to compute them with a finite element analysis. The quantities λ_1, λ_2 are easily obtained from knowledge of the surface normal n. In fact, since

$$\begin{aligned} n &= ((\nabla z)^T, 1)^T / ||((\nabla z)^T, 1)|| \\ &= ((\nabla z)^T, 1)^T / \sqrt{1 + z_x^2 + z_y^2} \end{aligned} \tag{3}$$

we get λ_2 by the z-component of the surface normal, and λ_1 by its inverse. Since the vertex normal's z-coordinate is less than its inverse, we view it as a heuristic approximation to the principal stress λ_2, and its inverse as one to λ_1. We expect the result of the topology optimization to be tightly linked to the magnitudes of the principal stresses, and therefore include the quantities (**??**) into the predictive model even though the chair's structure is not free of bending moment, and is therefore not in compression-only equilibrium.

4.1 Geometric Features for Statistical Learning

We were guided by searching for a possible correlation between the TO material density result and geometric features, as listed below.

1. Locally computable geometric features:
   - the principal curvatures κ_1, κ_2 as the most important local geometric features
   - the z-component of the surface's normal vector as well as its inverse, as motivated by the line of thoughts explained in Section **??**
   - the angles between the vertex normal and the direction of the applied load, for each of the applied loads (see Figure **??**)

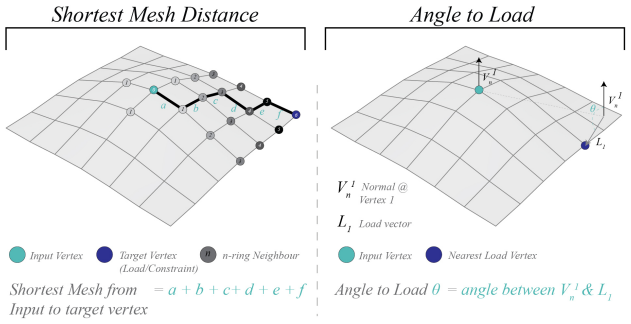

Figure 5. Calculating the Shortest Mesh Distance and Angle to Load

2. Simple globally computable features that are intuitively expected to have an impact on structure
   - the shortest mesh distance to constraint (see Figure **??**)
   - the shortest mesh distances to the closest load point, for each of the applied loads (see Figure **??**)

In total, our first model was one with nine linear features. In other words, the prediction was based on a *linear predictor* which is a linear combination of these nine features and a constant term called *intercept*. Moreover, we fitted a quadratic model, adding all possible quadratic terms to these , i.e., all two-fold products of any two features out of these, with the only exception being the product between the z-component and its inverse because it is equal to one and would therefore not add predictive value. Likewise, a cubic model incorporated all possible one-fold, two-fold and three-fold products of variables out of these nine variables.
For instance, the linear model featured linear combinations of the principal curvatures κ_1 and κ_2, and therefore made the mean curvature, the sum of κ_1 and κ_2, available as a predictive feature. The quadratic model, in turn, also incorporated the Gaussian curvature, the product of these two.
In total, there were $130 - 8 = 122$ predictors in the cubic model, including the intercept. Since the TO density results, obtained using the same TO setup explaind in Subsection **??**, were distributed on the unit interval $[0, 1]$ and therefore not normally distributed, linear regression had to be discarded. Instead, the density result had to be "*binned*" or "grouped". We applied a grouping threshold of 0.32, the median of the learning data's densities in such a way that both bins had the same size. For a refined analysis, the high density values were further subdivided into two groups of the same size, yielding three groups with the thresholds 0.32 and 0.63. Thus, there was a binary prediction target {low, high} and a three-class prediction target {low, middle, high}. For the former, we chose logistic regression, and for the latter ordinal logistic regression. We refer the reader to the vast statistical literature for introductions to these classical concepts, see for instance [**?**] as well as [**?**] and the references therein. For logistic regression, the prediction goal is binary, namely to discern between high and low topology-optimized values of the density D. In logistic regression, the prediction is based on the value of the linear predictor

$$\text{Prob}(D = \text{low}) = 1/\big(1+\exp(-(\beta_0 + \beta_1 X_1 + \beta_2 X_2 + \dots))\big), \tag{4}$$

where each X_i is a product of one, two or three features out of those described in Subsection **??**, β_0 is the intercept, and the β_i are the coefficients which are being fitted by the learning.
For multi-class prediction, we used an ordinal cumulative probability model ([**?**]). In it, one models the ordered stages of the discretized prediction target $D \in$ {low, middle, high} by means of the expression

$$\text{Prob}(D \le y) = \frac{\exp(\beta_0 - (\beta_1^y X_1 + \beta_2 X_2 + \dots))}{1 + \exp(\beta_0 - (\beta_1 X_1 + \beta_2 X_2 + \dots))}$$

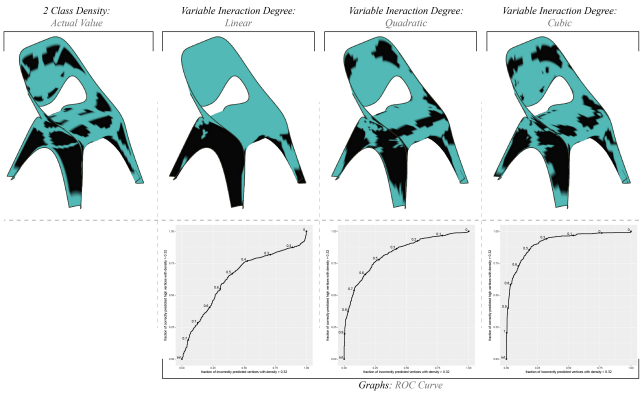

Figure 6. Predictions with Variable Interaction Degrees and corresponding ROC curves. The closer the ROC curve to the upper left corner, the better.

where $y \in \{\text{low, middle, high}\}$. Note that only the intercepts are assumed to depend on y. The coefficients β_i are to be estimated.

In order to prevent over-fitting, we strictly separated learning and testing geometries: models were either used for training or for testing, but not for both. Specifically, the geometry groups of Figure **??**A were used for learning the models, which were subsequently evaluated on the geometry groups of Figure **??**BCD.

4.2 Prediction Results

The prediction improved, as anticipated, when passing from the linear over the quadratic to the cubic model (Figure **??**). The evaluation of the model was done on the final chair's geometry.

Figure **??** contains predictions of the best model, the cubic model, on alternative geometry. Mostly, the geometric shape of the area formed by vertices with high density was accurately mapped. The model performed better in areas with highly variable geometry, such as the armrests, the backrest, and the legs, whereas in flat regions such as the seat, the prediction was weaker. The best prediction accuracy of up to 84% (i.e., the proportion of correctly classified vertices) was reached on the groups of Figure **??**BC which had only minor geometric deviations from training geometries of Figure **??**A. However, the geometries with larger geometric deviations of Figure **??**D had an accuracy of only 68% to 75%. Prediction with a logistic regression model with linear but without quadratic and cubic terms resulted in the coefficients given in Table 1 containing the coefficients β_i as defined in (**??**) in the first column. The second column indicates the p value, whose meaning is roughly described as the probability of observing such a high value of the corresponding coefficient by chance if the true coefficient was zero, i.e., if the corresponding variable had no real influence on the prediction target.

	Estimate	two-sided p-value
(Intercept)	-1.59	
κ_1	-0.02	$< 10^{-40}$
κ_2	0.02	$< 10^{-14}$
shortest mesh distance to constraint(SPC)	-0.66	$< 10^{-10}$
vertex normal z	-2.60	$< 10^{-32}$
shortest mesh distance to load S	0.28	$< 10^{-2}$
angle to load S	0.03	$< 10^{-20}$
shortest mesh distance to load BR	0.26	$< 10^{-3}$
angle to load HR	-0.003	$< 10^{-6}$
(vertex normal z)$^{-1}$	0.01	$< 10^{-8}$

Table 1. Estimated coefficients of the linear logistic model

Table 1 contains a few remarkable results. The magnitudes of the influences of κ_1 and κ_2 are the same but their signs are opposed to each other, implying that their difference has predictive value rather than their sum, the mean curvature. The influence of the shortest distance to the constraint is negative, implying that the density increases close to the constraint, as expected. The distances to the loads, however, have positive influence. The vertex normal's z-coordinate, the heuristic approximation to the second principal stress λ_2 has negative influence, its inverse has positive influence. All features are highly statistically significant (p-values < 0.05). The most powerful model, the cubic one, however, is harder to interpret since in it, each variable occurs often, in different products.

5 FUTURE WORKS

The objective of using TO in the early design work-flow, production of geometry for multi-color 3D-printing and finding correlation between geometric features and TO density results using statistical learning were successful. However issues raised and results obtained during these processes have scope for development under the domains explained below.

Automation of Re-meshing

The process of re-meshing (Subsection **??**) is currently done manually. We propose to develop on research of *skeletal extraction* [**?**] to automate the process of extraction of skeletal mesh based on the TO results.

3D-Printing

The current production process prohibits the usage of smooth gradients, due to the limited number of colors available in the material color catalog [**?**]. The constraints of the printer provided by Stratasys also governed the use of constant material properties for the production shells in the 3D-printed prototypes. We propose to build on research of *voxel based/ data driven material* [**?**] as a transfer of production information with the printer in order to create smooth gradients in color and multi-material prints. Our design work flow incorporating TO is easily amenable to generate data on material property variation based on structural results.

Statistical learning of structural properties

The current prediction performs reasonably well as long as the learning and the predicting geometries remain within a given series of related geometries. It would be worthwhile to study ways of expanding the prediction radius to more distant or distorted geometries than those the model was learned on. In that vein, we envisage to add further co-variables to those enumerated in Subsection **??** in order to improve the prediction. To be more precise, let us recall that the coefficients of the higher order terms indicate the best-fit description of the surface in terms of the graph of polynomials of higher degree [**?**]. These coefficients provide good candidates for further locally computable geometric features that are empirically correlated with structural features.

Another venue for future work is the challenge to predict the

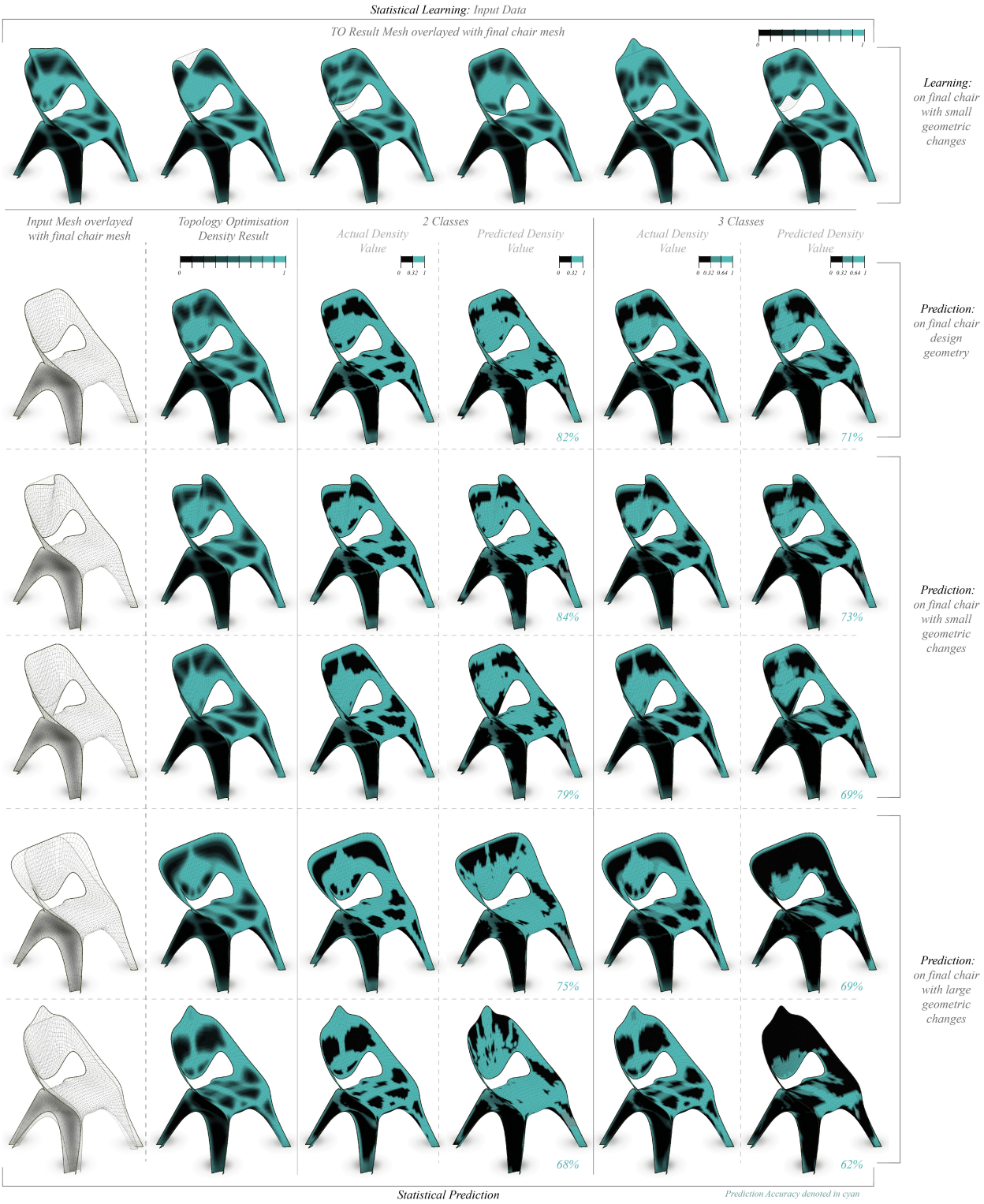

Figure 7. Statistical Learning and Prediction Results

Figure 8. 3D-Printed Chair Prototypes

principal stress directions. In a first step, it is possible to derive an immediate good guess of the principal stress direc-

tions on funicular surfaces, along the lines developed in Section **??**. The approximation might be improved by finding better ways of local guesses of the Airy function associated with the geometry and the loading conditions, thereby implying the stress tensor field.

6 CONCLUSION

We have documented a TO-driven design process, and generated production information for a multi-color 3D-Print (Figure **??**). In addition, we have described a novel method of approximating TO results using statistical learning, which opens up further avenues for research. These are the key contributions of this paper.

ACKNOWLEDGMENTS

This research was carried out with the support and guidance of Zaha Hadid Architects, especially Patrik Schumacher. We would like to thank Stratasys, our research collaborator and technical support on 3D-printing, and Altair for technical support on Hypermesh.